POWER BEACON-ASSISTED ENERGY HARVESTING IN D2D NETWORK UNDER CO-CHANNEL INTERFERENCES: SYMBOL ERROR RATE ANALYSIS

Nguyen Quang Sang¹, Tran Cong Hung², Ngoc-Long Nguyen³, Bui Vu Minh⁴ and Lubos Rejfek⁵

(Received: 15-Aug.-2025, Revised: 15-Oct.-2025, Accepted: 1-Nov.-2025)

ABSTRACT

This paper studies the symbol error rate (SER) performance of a wireless-powered device-to-device (D2D) communication system operating under a time-switching (TS) protocol in the presence of multiple co-channel interferers (CCI). The considered model involves a battery-less source harvesting energy from multiple dedicated power beacons and transmitting to a multi-antenna destination over quasi-static Rayleigh fading channels. Both selection combining (SC) and maximal ratio combining (MRC) schemes are examined at the destination. In addition to the SER analysis, the outage probability (OP) performance is also investigated based on the derived cumulative distribution functions (CDFs), providing a complementary perspective on system reliability. The analysis focuses on the impact of key system parameters, including the interference power level, interferer-to-destination distance, energy harvesting efficiency, and modulation type, on the overall performance. Comprehensive simulation results are presented to validate the analytical derivations and to demonstrate the effects of these parameters on both SER and OP. The obtained results offer valuable insights into the design of energy-constrained D2D systems operating in spectrum-sharing environments, serving as a reference for future enhancements and practical deployments.

KEYWORDS

Co-channel interference, Energy harvesting, Device-to-device, Symbol error rate.

1. Introduction

The Internet of Things (IoT) has emerged as a groundbreaking paradigm, enabling seamless interconnection between physical objects, sensors, and digital systems, allowing them to collect, process, and exchange data with minimal human intervention [1,2,3]. With the rapid development of smart cities, intelligent transportation, environmental monitoring, and industrial automation, IoT networks have become an indispensable part of modern life. The evolution toward fifth-generation (5G) and upcoming sixth-generation (6G) wireless networks promises ultra-reliable communications, low latency, massive device connectivity, and ubiquitous coverage, further accelerating IoT adoption [4, 5, 6]. However, the large number of IoT devices poses a significant challenge - most of these devices are powered by batteries with limited energy-storage capacity [7]-[8]. In many applications, such as remote sensing, underground monitoring, or post-disaster recovery scenarios, replacing or recharging batteries is impractical, costly, or even impossible. Therefore, ensuring long-term network operation without manual intervention has become a key research direction.

In this context, Wireless Power Transfer (WPT) has emerged as a promising technology to address the challenge of limited battery life in future wireless networks, especially for the large-scale deployment of low-power IoT devices. By leveraging Energy Harvesting (EH) techniques, wireless network nodes can capture energy from ambient radio frequency (RF) signals or dedicated power sources, thereby enabling sustainable operation without frequent battery replacement [9], [10]. This has motivated a large body of research focused on analyzing, evaluating, and optimizing the performance of EH-enabled systems in various communication scenarios. Several works have examined specific network models

^{1.} N. Q. Sang is with the Posts and Telecommunications Institute of Technology, Ho Chi Minh City, Vietnam. Email: sangnq@ptit.edu.vn

^{2.} T. C. Hung is with the School of Computer Science & Engineering, The SaiGon International University, Ho Chi Minh City, Vietnam. Email: tranconghung@siu.edu.vn

^{3.} N.-L. Nguyen (Corresponding Author) is with the Faculty of Applied Sciences, Ton Duc Thang University, Ho Chi Minh City, Vietnam. Email: nguyenngoclong@tdtu.edu.vn

^{4.} B. V. Minh is with the Faculty of Engineering and Technology, Nguyen Tat Thanh University, Ho Chi Minh City, Vietnam. Email: bvminh@ntt.edu.vn

L. Rejfek is with the Faculty of Electrical Engineering and Informatics, University of Pardubice, 53210 Pardubice, Czech Republic. Email: Lubos.Rejfek@upce.cz

supported by dedicated power beacons. For instance, [9] analyzes the outage performance of a symbiotic radio network assisted by a power beacon, thereby clarifying the impact of energy harvesting on datatransmission capability. Similarly, [10] investigates physical layer security in IoT networks with multiple power beacons, evaluating the secrecy outage probability (SOP) under different energy configurations. For large-scale IoT networks, [11] employs stochastic geometry to analyze the coverage probability of EH-enabled LoRa networks, shedding light on the effects of node density, spatial distribution, and signal strength on connectivity. Beyond terrestrial networks, EH has also been integrated into unmanned aerial vehicle (UAV) communications, where energy supply is a severe limiting factor. [12] reveals the inherent trade-off between reliability and security in UAV systems supported by EH relays, providing design guidelines to balance these two objectives. In the field of nonorthogonal multiple access (NOMA), [13] analyzes the uplink and downlink performance of EH-enabled NOMA systems, providing exact expressions for throughput and outage probability (OP). Extending further, [14] proposes a statistical model for the sum of double random variables and applies it to optimize the performance of NOMA systems assisted by simultaneous transmitting and reflecting reconfigurable intelligent surfaces (STAR-RIS), demonstrating their capability to enhance EH system efficiency and flexibility. Furthermore, physical layer security has also been a central focus in EH research. The work in [15] introduces a friendly jammer to improve security in wireless sensor networks while analyzing the SOP. Similarly, [16] investigates a self-energy recycling model in full-duplex decode-and-forward (DF) relay networks, jointly evaluating security and reliability. In another direction, [17] investigates the performance of an EH full-duplex relay system employing multi-antenna techniques and cooperative diversity. It analyzes key metrics, such as outage probability and bit error rate under various fading conditions using transmit-antenna selection, maximal-ratio combining, and power splitting schemes. Moreover, [18] provides exact and upper-bound capacity analysis for fullduplex DF EH networks with a hybrid time power switching relaying (TPSR) protocol, establishing the theoretical foundation for protocol optimization. In addition to long-packet systems, [19] focuses on short-packet communication (SPC) in EH-enabled IoT networks, where latency and reliability become critical determinants of system performance. With its outstanding benefits in energy sustainability, performance enhancement, and security support, EH is becoming an indispensable component in the design and optimization of modern wireless networks.

In addition to sustaining long-term operation, IoT and 5G/6G networks also demand communication mechanisms that offer flexibility, spectral efficiency, and high reliability. Among these, Device-to-Device (D2D) communication is a key enabling technology, allowing nearby user pairs to connect directly without routing through a base station (BS). This mechanism reduces latency, improves spectral efficiency, alleviates cellular network load, and enhances both energy efficiency and system throughput [20], [21]. Depending on spectrum usage, D2D can operate in in-band mode - sharing licensed spectrum with cellular users - or out-band mode - utilizing unlicensed spectrum [20], [21]. Among these, in-band underlay D2D has been extensively studied due to its efficient spectrum reuse, although it requires strict control over interference caused to cellular networks. For example, [22] analyzes the OP, average rate, and amount of fading (AoF) of underlay D2D networks under three different power-allocation strategies, showing that path-loss-based allocation outperforms equal or random allocation. For energy-constrained devices, EH has been integrated into D2D as a promising solution. [23] proposes a D2D model supported by a power beacon and cooperative jamming from multiple nodes to enhance physical layer security, providing closed-form expressions for OP, intercept probability (IP), and SOP. Moreover, [24] combines partial NOMA with backscatter communication (BackCom) to improve both energy and spectral efficiency in D2D, deriving closed-form OP expressions over Rayleigh fading channels. Relayaided D2D has also received strong attention for its ability to extend coverage and improve reliability in both one-way relaying (OWR) and two-way relaying (TWR) modes [25]. Research shows that resource allocation, relay selection, and power optimization should be integrated with EH and machinelearning (ML) algorithms to achieve superior performance [25], [26]. In resource optimization, methods such as bee-colony optimization [27] or distributed resource allocation based on reinforcement learning (RL) [26] have proven effective in improving throughput, spectral efficiency, and fairness. Meanwhile, security remains a major challenge due to the direct connectivity of D2D. [28] provides a comprehensive analysis of security threats, such as eavesdropping, spoofing, and jamming attacks, while proposing a security architecture for next-generation D2D systems. In the IoT context, [29] presents a multi-criteria learning algorithm using security sensors to maintain data reliability and integrity in smart environments with D2D support. The potential of D2D is further enhanced when combined with emerging

technologies, such as reconfigurable intelligent surfaces (RIS) and NOMA [30], which enable optimization of the propagation environment and improvement of link quality, while analyzing OP under imperfect interference-cancellation conditions.

However, both D2D and EH systems deployed in high-spectrum reuse environments must contend with co-channel interference (CCI), one of the main sources of interference in wireless communication systems.

CCI arises when multiple links share the same frequency channel, which can significantly degrade received-signal quality, leading to higher error rates, reduced throughput and compromised system reliability. With the increasing network density and aggressive frequency reuse in technologies, such as 5G, IoT, and satellite networks, analyzing and mitigating the impact of CCI has become an important research direction to ensure optimal system performance. Recent works have investigated the presence of CCI in various wireless communication scenarios. In [31], CCI at the relay node is considered in a cooperative SPC system with transmit-antenna selection and beamforming, analyzing the block error rate (BLER) and proposing an optimal power allocation strategy. [32] extends the SPC analysis to single-hop systems with CCI at the destination, providing exact and asymptotic closed-form expressions for BLER. In the IoT domain, [35] investigates a two-way relaying NOMA (TWR-NOMA) system with a power beacon, analyzing the effects of CCI on OP, throughput, and ergodic capacity and incorporating optimization and deep-learning techniques to improve performance. In addition, [33] analyzed the performance of EH-enabled D2D systems under co-channel interference, while [34] investigated the outage probability and error rate of wireless-powered communication networks operating in interference-limited environments, emphasizing the impact of energy-harvesting efficiency and interference power on system reliability.

In summary, with the rapid development of advanced wireless communication techniques, such as EH, diversity combining, and interference management, the performance of many current systems has been significantly improved in terms of reliability, energy efficiency, and interference resilience. Numerous recent studies have contributed to this progress by investigating various network architectures and operating conditions. For instance, several recent works have provided new insights into energyharvesting (EH) and interference-limited systems under different scenarios. Specifically, [45] investigated the physical layer security of EH-enabled IoT networks with hardware impairments, while [46] analyzed outage and throughput performance in backscatter-assisted SWIPT systems. [47] presented a secure and covert communication framework for energy-harvesting relay IoT networks, while [48] examined the joint optimization of resource allocation and energy efficiency in STAR-RISassisted networks. In addition, [49] explored the outage behavior of NOMA-enabled UAV systems under imperfect channel conditions, whereas [50] analyzed short-packet transmissions for EH-based IoT systems considering reliability-latency trade-offs. Meanwhile, [35] proposed and evaluated a PB- and NOMA-assisted cooperative IoT network under CCI, while [36] analyzed the outage performance of satellite-terrestrial full-duplex relaying networks with CCI and further applied deep learning for performance prediction. [37] examined the outage probability of an EH-based cooperative NOMA network with a direct link, whereas [38] presented performance analysis and optimal design of a timeswitching EH protocol for MIMO full-duplex DF relay networks employing different diversity techniques. Similarly, [39] exploited the direct link in two-way half-duplex sensor networks over block Rayleigh fading to derive an upper bound of the ergodic capacity and provide an exact SER analysis. The impact of CCI has also been investigated in other contexts, such as IRS-assisted communications [40], multisource cooperative networks assisted by UAV relays [41] and dual-hop mixed RF/FSO relaying systems with both CCI and pointing errors [42]. Moreover, [43] addressed short-packet communications for relay systems with CCI at the relay, offering performance analysis and powercontrol strategies, while [44] explored the second-order statistics for IRS-assisted multi-user vehicular networks with CCI. However, despite these advancements, our literature survey reveals a lack of comprehensive studies that evaluate the performance of systems simultaneously integrating PB-assisted EH, multi-antenna diversity reception and the effects of CCI-particularly when combining both selection combining (SC) and maximal ratio combining (MRC) techniques. Motivated by this research gap, we propose a unified system model in which an energy-constrained source node harvests energy from a PB to transmit information to a multi-antenna destination in the presence of multiple CCI sources. Furthermore, to provide a more comprehensive evaluation, the study focuses on analyzing and computing the symbol error rate (SER) under both SC and MRC techniques, thereby offering deeper insights into the impact of interference and the effectiveness of each diversity-reception method. In the context of increasingly scarce spectrum resources and the inevitable interference from existing wireless systems, analyzing and optimizing system performance under such conditions holds both scientific significance and practical value.

The main contributions of this paper can be summarized as follows:

- This work investigates the impact of co-channel interference (CCI) on the performance of wireless-powered D2D systems, where a batteryless source harvests energy from dedicated power beacons (PBs) and utilizes this harvested energy to communicate with a multi-antenna destination in the presence of multiple interferers.
- The analysis includes both the symbol error rate (SER) and the outage probability (OP) performance under two receive combining techniques at the destination; namely, selection combining (SC) and maximal ratio combining (MRC). New closed-form expressions for both SER and OP are derived, capturing the effects of multiple interference sources and various key system parameters.

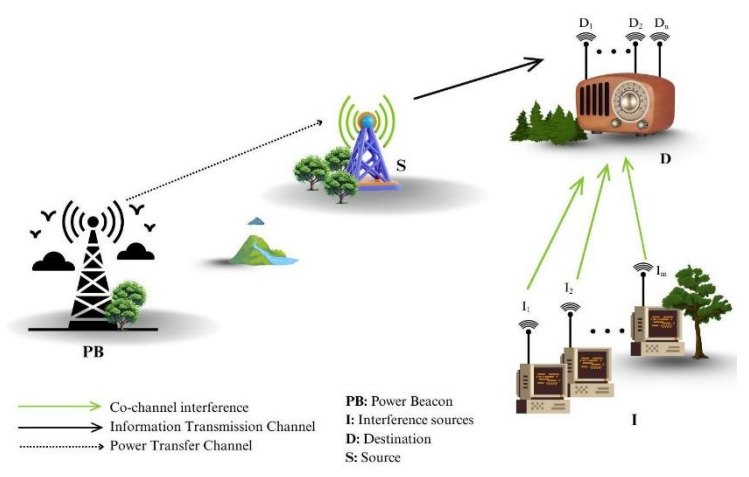


Figure 1. System model.

• Extensive numerical and Monte Carlo simulation results are provided to validate the analytical derivations. The results offer valuable design insights into the trade-offs between reliability and energy efficiency, revealing, for instance, the performance advantage of MRC over SC, the influence of energy-harvesting efficiency on both SER and OP and the sensitivity of system performance to interference power levels.

ble 1. Compa	ırıson o	of the u	niquenes	s of our research	to relat	ed artic
Context	EH	SC	MRC	Multi-antenna	CCI	SER
Paper [17]	✓	✓	√	✓		✓
Paper [35]	✓				✓	
Paper [37]	√	✓	√			
Paper [38]	✓		√	✓		
Paper [39]	✓					✓
Paper [40]				✓	✓	
Paper [41]		✓	√		✓	
Paper [42]		✓	√		✓	✓
Paper [43]		✓	√		✓	
Paper [44]				✓	✓	
This paper	✓	√	✓	✓	✓	✓

Table 1. Comparison of the uniqueness of our research to related articles.

The remainder of the paper is organized as follows. Section 2 gives an overview of the system model. Section 3 presents the information-theoretic mathematical framework, guiding on how to achieve the SER. Section 4 presents numerical results and discussions to validate the developed framework as well as deeply explore the impacts of system key parameters, while Section 5 provides concluding remarks.

2. SYSTEM MODEL

We consider a wireless-powered D2D communication system, as illustrated in Fig. 1, where a batteryless source node *S* communicates with a multi-antenna destination node *D* in the presence of multiple cochannel interferers. The source harvests energy from a dedicated power beacon (P) during the EH phase and then reuses this harvested energy to transmit information to the destination in the information-transmission phase, following the time-switching (TS) protocol depicted in Fig. 2. The system operates over a quasi-static flat Rayleigh fading environment, where channel coefficients remain constant during each transmission block, but vary independently between blocks. In addition to the intended signal, the destination also receives undesired signals from *M* interfering transmitters operating on the same frequency band, which cause CCI. Such a setting captures a realistic scenario in spectrum-constrained environments, where D2D communications coexist with other wireless systems and must operate under both energy limitations and interference conditions.

Let us denote h_{PS} , h_{SD_n} , h_{I_mD} as channel coefficients of the direct link from source node P to destination node D, and P \rightarrow S, S \rightarrow D_n, I_m \rightarrow D, links, respectively. Assume that h_X , X \in {PS, SD_n, I_mD} are Rayleigh fading channels, channel gains $\gamma_X = |h_X|^2$ are exponential random variables (RVs) whose probability density function (PDF) and cumulative distribution function (CDF) are given as, respectively.

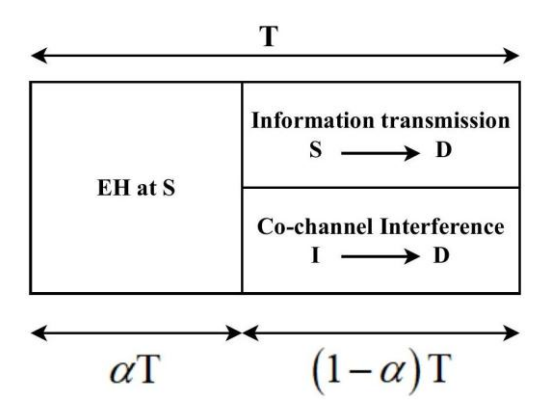


Figure 2. Time switching.

$$f_{\gamma_{X}}(x) = \lambda_{X} \exp(-\lambda_{X} x)$$

$$F_{\gamma_{X}}(x) = 1 - \exp(-\lambda_{X} x)$$
(1)

where λ_X is the mean of γ_X . To consider a simple-path loss model, λ_X can be modeled by $\lambda_X = (d_X)^{\chi}$, where d_X is the distance between two correspondence nodes and χ is the path-loss exponent. In the energy-harvesting phase, firstly S will harvest the energy from P and then, energy at S can be expressed as:

$$E_{S} = \eta \alpha T P_{P} \gamma_{PS} \tag{2}$$

Then, the transmit power of S can be formulated as:

$$P_{S} = \frac{E_{S}}{(1-\alpha)T} = \frac{\eta \alpha P_{P} \gamma_{PS}}{(1-\alpha)} = \kappa P_{P} \gamma_{PS}$$
 (3)

where,
$$\kappa = \frac{\eta \alpha}{(1-\alpha)}$$

In the data-transmission phase, S transmits unit power signals x_S to the nth D; i.e., n^{th} , where $E\{|x_S|^2\} = 1$ is the expectation operator.

The received signal at n^{th} D is given as follows:

"Power Beacon-assisted Energy Harvesting in D2D Network under Co-channel Interferences: Symbol Error Rate Analysis", N.Q. Sang et.al.

$$y_{\mathrm{D}_{n}} = \underbrace{\sqrt{P_{\mathrm{S}}} h_{\mathrm{SD}_{n}} x_{\mathrm{S}}}_{\text{signal}} + \underbrace{\sqrt{P_{\mathrm{I}}} \sum_{m=1}^{M} h_{\mathrm{I}_{m} \mathrm{D}} x_{\mathrm{I}_{m}}}_{\text{noise}} + n_{\mathrm{D}_{n}} \underbrace{+ n_{\mathrm{D}_{n}}}_{\text{noise}}$$
(4)

where n_{D_n} is the AWGN with zero mean and variance N_0 . The received signal-to-noise ratio (SNR) at the n^{th} D in this phase can be thus calculated by:

$$\gamma_{\mathrm{D}_n} = \sqrt{\frac{\mathrm{E}\{|\mathrm{signal}|^2\}}{\mathrm{E}\{|\mathrm{interference}|^2\} + \mathrm{E}\{|\mathrm{noise}|^2\}}} = \frac{P_{\mathrm{S}}\gamma_{\mathrm{SD}_n}}{P_{\mathrm{I}}\gamma_{\mathrm{ID}} + N_0}$$
 (5)

where $\gamma_{\text{ID}} = \sum_{m=1}^{M} |h_{\text{I}_m \text{D}}|^2$.

Using the fact that $N_0 \ll P_{\rm I}$, then by doing some algebra, by substituting (3) into (5), we have:

$$\gamma_{\mathrm{D}_n} = \frac{\kappa P_{\mathrm{P}} \gamma_{\mathrm{PS}} \gamma_{\mathrm{SD}_n}}{P_{\mathrm{I}} \gamma_{\mathrm{ID}} + N_0} \approx \frac{\kappa \Psi_{\mathrm{P}} \gamma_{\mathrm{PS}} \gamma_{\mathrm{SD}_n}}{\Psi_{\mathrm{I}} \gamma_{\mathrm{ID}}}$$
(6)

where $\Psi_P = \frac{P_I}{N_0}$; $\Psi_I = \frac{P_I}{N_0}$. In order to make the paper highly applicable, we examine two situations using various diversity technique:

1. Scenario 1: In the first considered scenario, the destination node *D* employs the SC technique to process the received signals from its multiple antennas[51]. Specifically, *D* selects the antenna branch with the highest instantaneous signal-to-interference-plus-noise ratio (SINR) for detection, while discarding the other branches. Therefore, the resulting SINR at *D* can be expressed as:

$$\gamma_{\rm D}^{\rm SC} = \frac{\kappa \Psi_{\rm P} \gamma_{\rm PS} \gamma_{\rm SD}^{\rm SC}}{\Psi_{\rm I} \gamma_{\rm ID}} \tag{7}$$

where $\gamma_{\text{SD}}^{\text{SC}} = \max_{1 \leqslant n \leqslant N} \left[\left| h_{\text{SD}_n} \right|^2 \right]$.

2. Scenario 2: In the second scenario, the destination node *D* adopts the MRC technique to exploit all available antenna branches [52]. In this method, the received signals at different antennas are coherently combined after being weighted according to their respective channel gains, thereby maximizing the overall SINR at *D*. Therefore, the resulting SINR at *D* can be expressed as:

$$\gamma_{\rm D}^{\rm MRC} = \frac{\kappa \Psi_{\rm P} \gamma_{\rm PS} \gamma_{\rm SD}^{\rm MRC}}{\Psi_{\rm I} \gamma_{\rm ID}} \tag{8}$$

where $\gamma_{\text{SD}}^{\text{MRC}} = \sum_{n=1}^{N} |h_{\text{SD}_n}|^2$

3. Performance Analysis

3.1 CDF and PDF Derivation

3.1.1 CDF and PDF of γ_{SD}^{SC} , γ_{SD}^{MRC}

Based on [53], the CDF and PDF can be found as, respectively:

$$F_{\gamma_{\text{SD}}C}(x) = 1 - \sum_{n=1}^{N} {N \choose n} (-1)^{n-1} \exp(-n\lambda_{\text{SD}}x),$$

$$f_{\gamma_{\text{SD}}^{\text{SC}}}(x) = \sum_{n=1}^{N} {N \choose n} \times n\lambda_{\text{SD}}(-1)^{n-1} \exp(-n\lambda_{\text{SD}}x),$$
(9)

$$F_{\xi}(x) = \frac{1}{\Gamma(N)} \gamma(N, \lambda_k x)$$

$$f_{\xi}(x) = \frac{(\lambda_{SD})^N}{\Gamma(N)} x^{N-1} \exp(-\lambda_k x)$$
(10)

where $\Gamma(\cdot)$ is the Gamma function, as defined in section (8.31) of reference [54], $\xi \in \{\gamma_{SD}^{MRC}, \gamma_{ID}\}$, and $k \in \{SD, ID\}$.

3.1.2 CDF of γ_D^{SC}

$$F_{\gamma_{\rm D}^{\rm SC}}(x) = \Pr(\gamma_{\rm D}^{\rm SC} < x) \tag{11}$$

By substituting (7) into (11), we obtain:

$$F_{\gamma_{\rm D}^{\rm SC}}(x) = \Pr(\frac{\kappa \Psi_{\rm P} \gamma_{\rm PS} \gamma_{\rm SD}^{\rm SC}}{\Psi_{\rm I} \gamma_{\rm ID}} < x)$$

$$= \int_0^{+\infty} \int_0^{+\infty} F_{\gamma_{\rm PS}}(\frac{x \Psi_{\rm I} z}{\kappa \Psi_{\rm P} y}) f_{\gamma_{\rm SD}^{\rm SC}}(y) f_{\gamma_{\rm ID}}(z) dy dz$$
(12)

By substituting (9) into (12), we obtain:

$$F_{\gamma_{\rm D}^{\rm SC}}(x) = \int_0^{+\infty} \int_0^{+\infty} F_{\gamma_{\rm PS}}(\frac{x\Psi_{\rm I}z}{\kappa\Psi_{\rm P}y}) f_{\gamma_{\rm SD}^{\rm SC}}(y) f_{\gamma_{\rm ID}}(z) dy dz$$

$$= 1 - \int_0^{+\infty} \left\{ \exp(\frac{-\lambda_{\rm PS}x\Psi_{\rm I}z}{\kappa\Psi_{\rm P}y}) \sum_{n=1}^N \binom{N}{n} \times n\lambda_{\rm SD}(-1)^{n-1} \exp(-n\lambda_{\rm SD}y) \right\} dy dz$$

$$\times \frac{(\lambda_{\rm ID})^M}{\Gamma(M)} z^{M-1} \exp(-\lambda_{\rm ID}z)$$

$$(13)$$

Based on [54] [Eq: 3.324 and 6.643-3], (13) can be figured out as:

$$F_{\gamma_{D}^{SC}}(x) = 1 - \int_{0}^{+\infty} \int_{0}^{+\infty} \exp\left(\frac{-\lambda_{PS}x\Psi_{I}z}{\kappa\Psi_{P}y}\right) \sum_{n=1}^{N} {N \choose n} \times n\lambda_{SD}(-1)^{n-1} \exp(-n\lambda_{SD}y)$$

$$\times \frac{(\lambda_{ID})^{M}}{\Gamma(M)} z^{M-1} \exp(-\lambda_{ID}z)$$

$$= 1 - \sum_{n=1}^{N} {N \choose n} \Gamma(M+1)(-1)^{n-1} \exp\left(\frac{n\lambda_{PS}\lambda_{SD}x\Psi_{I}}{2\kappa\Psi_{P}\lambda_{ID}}\right) \times W_{-M,\frac{1}{2}} \left(\frac{n\lambda_{PS}\lambda_{SD}x\Psi_{I}}{\kappa\Psi_{P}\lambda_{ID}}\right)$$

$$(14)$$

where $W(\cdot)$ is the Whittaker function, as defined in section. (9.22) of reference [54].

3.1.3 CDF of γ_D^{MRC}

$$F_{\gamma_{\rm D}^{\rm MRC}}(x) = \Pr(\gamma_{\rm D}^{\rm MRC} < x) \tag{15}$$

By substituting (8) into (15), we obtain:

$$F_{\gamma_{\rm D}^{\rm MRC}}(x) = \Pr(\frac{\kappa \Psi_{\rm P} \gamma_{\rm PS} \gamma_{\rm SD}^{\rm MRC}}{\Psi_{\rm I} \gamma_{\rm ID}} < x)$$

$$= \int_0^{+\infty} \int_0^{+\infty} F_{\gamma_{\rm PS}}(\frac{\kappa \Psi_{\rm I} z}{\kappa \Psi_{\rm P} y}) f_{\gamma_{\rm SD}^{\rm MRC}}(y) f_{\gamma_{\rm ID}}(z) dy dz$$
(16)

By substituting (1) and (10) into (16), we claim:

$$F_{\gamma_{\mathrm{D}}^{\mathrm{MRC}}}(x) = \int_{0}^{+\infty} \int_{0}^{+\infty} F_{\gamma_{\mathrm{PS}}}(\frac{x\Psi_{\mathrm{I}}z}{\kappa\Psi_{\mathrm{P}}y}) f_{\gamma_{\mathrm{SD}}^{\mathrm{MRC}}}(y) f_{\gamma_{\mathrm{ID}}}(z) dy dz$$

$$= 1 - \int_{0}^{+\infty} \left\{ \exp(\frac{-\lambda_{\mathrm{PS}}x\Psi_{\mathrm{I}}z}{\kappa\Psi_{\mathrm{P}}y}) \frac{(\lambda_{\mathrm{SD}})^{N}}{\Gamma(N)} y^{N-1} \exp(-\lambda_{\mathrm{SD}}y) \right\} dy dz$$

$$\times \frac{(\lambda_{\mathrm{ID}})^{M}}{\Gamma(M)} z^{M-1} \exp(-\lambda_{\mathrm{ID}}z)$$

$$(17)$$

Based on [54] Eq: 3.471-9 and Eq: 6.643-3, (17) can be figured out as:

$$F_{\gamma_{\rm D}^{\rm MRC}}(x) = 1 - \frac{\Gamma(M+N)}{\Gamma(N)} \left(\frac{\lambda_{\rm SD}\lambda_{\rm PS}x\Psi_{\rm I}}{\kappa\Psi_{\rm P}\lambda_{\rm ID}}\right)^{\frac{N-1}{2}} \times \exp\left(\frac{\lambda_{\rm SD}\lambda_{\rm PS}x\Psi_{\rm I}}{2\kappa\Psi_{\rm P}\lambda_{\rm ID}}\right) \times W_{-M-\frac{N}{2}+\frac{1}{2}\frac{N}{2}} \left(\frac{\lambda_{\rm SD}\lambda_{\rm PS}x\Psi_{\rm I}}{\kappa\Psi_{\rm P}\lambda_{\rm ID}}\right)$$
(18)

"Power Beacon-assisted Energy Harvesting in D2D Network under Co-channel Interferences: Symbol Error Rate Analysis", N.Q. Sang et.al.

3.2 Outage-probability (OP) Analysis

The OP of the system can be thus defined by:

$$OP^{\varpi} = \begin{cases} Pr(\gamma_{D}^{SC} < \gamma_{th}), \varpi = SC \\ Pr(\gamma_{D}^{MRC} < \gamma_{th}), \varpi = MRC \end{cases}$$
 (19)

where $\gamma_{th}\,=2^{R_{th}}\,-1$ is the threshold of the system and $R_{th}\,$ is the target rate.

3.2.1 Scenario 1: SC Technique Is Employed at the Destination

The OP for Scenario 1 is given as follows:

$$OP^{SC} = Pr(\gamma_D^{SC} < \gamma_{th}) \tag{20}$$

Based on (11) and (14) and by substituting $x = \gamma_{th}$ into (20), we have:

$$OP^{SC} = 1 - \sum_{n=1}^{N} {N \choose n} \Gamma(M+1) (-1)^{n-1} \exp\left(\frac{n\lambda_{PS}\lambda_{SD}\gamma_{th}\Psi_{I}}{2\kappa\Psi_{P}\lambda_{ID}}\right) \times W_{-M,\frac{1}{2}} \left(\frac{n\lambda_{PS}\lambda_{SD}\gamma_{th}\Psi_{I}}{\kappa\Psi_{P}\lambda_{ID}}\right)$$
(21)

3.2.2 Scenario 2: MRC Technique Is Employed at the Destination

The OP for Scenario 2 is given as follows:

$$OP^{MRC} = Pr(\gamma_D^{MRC} < \gamma_{th})$$
 (22)

Based on (15) and (18) and by substituting $x = \gamma_{th}$ into (22), we have:

$$OP^{MRC} = 1 - \frac{\Gamma(M+N)}{\Gamma(N)} \left(\frac{\lambda_{SD} \lambda_{PS} \gamma_{th} \Psi_{I}}{\kappa \Psi_{P} \lambda_{ID}} \right)^{\frac{N-1}{2}} \times \exp\left(\frac{\lambda_{SD} \lambda_{PS} \gamma_{th} \Psi_{I}}{2\kappa \Psi_{P} \lambda_{ID}} \right) \times W_{-M - \frac{N}{2} + \frac{1}{2} \frac{N}{2}} \left(\frac{\lambda_{SD} \lambda_{PS} \gamma_{th} \Psi_{I}}{\kappa \Psi_{P} \lambda_{ID}} \right)$$
(23)

3.3 Symbol Error Ratio (SER) Analysis

Based on [39], SER can be defined as:

$$SER = E\left\{aQ\left(\sqrt{2b\gamma_{\rm D}^{\zeta}}\right)\right\} \tag{24}$$

where $\zeta \in (SC, MRC)$, $Q(t) = \frac{1}{\sqrt{2\pi}} \int_t^{+\infty} e^{-x^2/2} dx$ is the Gaussian Q-function [55], while a and b are constants, which are specific for each modulation; (a,b)=(1,1) for binary phase-shift keying (BPSK) and (a,b)=(1,2) for Quadrature Phase Shift Keying (QPSK). As a result, before obtaining the SER performance, the CDF of γ_D^{ζ} is adopted. Then, Equation (24) can be reformulated as follows:

SER =
$$\frac{a\sqrt{b}}{2\sqrt{\pi}} \int_0^{+\infty} \frac{e^{-bx}}{\sqrt{x}} \times F_{\gamma_D^{\zeta}}(x) dx$$
 (25)

3.3.1 Scenario 1: SC Technique Is Employed at the Destination

In this scenario, by substituting (14) into (25), the SER can be analyzed as:

$$\operatorname{SER}_{D}^{SC} = \frac{a\sqrt{b}}{2\sqrt{\pi}} \int_{0}^{+\infty} \frac{e^{-bx}}{\sqrt{x}} \times \left\{ 1 - \sum_{n=1}^{N} \binom{N}{n} \Gamma(M+1)(-1)^{n-1} \\ \exp\left(\frac{n\lambda_{PS}\lambda_{SD}x\Psi_{I}}{2\kappa\Psi_{P}\lambda_{ID}}\right) \times W_{-M,\frac{1}{2}} \frac{n\lambda_{PS}\lambda_{SD}x\Psi_{I}}{\kappa\Psi_{P}\lambda_{ID}}\right\} dx$$

$$= \underbrace{\frac{a\sqrt{b}}{2\sqrt{\pi}} \int_{0}^{+\infty} \frac{e^{-bx}}{\sqrt{x}} dx - \underbrace{\frac{a\sqrt{b}}{2\sqrt{\pi}} \sum_{n=1}^{N} \binom{N}{n} \Gamma(M+1)(-1)^{n-1} \int_{0}^{+\infty} \frac{1}{\sqrt{x}} \frac{e^{-bx}(\frac{n\lambda_{PS}\lambda_{SD}x\Psi_{I}}{2\kappa\Psi_{P}\lambda_{ID}} - bx)}{\frac{N}{2\sqrt{x}} \left(\frac{n\lambda_{PS}\lambda_{SD}x\Psi_{I}}{2\kappa\Psi_{P}\lambda_{ID}}\right)} dx$$

$$\Phi_{2} \qquad (26)$$

From (26), and after applying [54][Eq: 3.361.2], Φ_1 can be calculated as:

$$\Phi_1 = \frac{a\sqrt{b}}{2\sqrt{\pi}} \int_0^{+\infty} \frac{e^{-bx}}{\sqrt{x}} dx = \frac{a}{2}$$
 (27)

Next, Φ_2 is expressed by:

$$\Phi_{2} = \frac{a\sqrt{b}}{2\sqrt{\pi}} \sum_{n=1}^{N} {N \choose n} \Gamma(M+1) (-1)^{n-1} \int_{0}^{+\infty} \frac{\frac{1}{\sqrt{x}} \exp(\frac{n\lambda_{PS}\lambda_{SD}x\Psi_{I}}{2\kappa\Psi_{P}\lambda_{ID}} - bx)}{\sqrt{x}W_{-M,\frac{1}{2}} (\frac{n\lambda_{PS}\lambda_{SD}x\Psi_{I}}{\kappa\Psi_{P}\lambda_{ID}})} dx$$

$$= \frac{a\sqrt{b}}{2\sqrt{\pi}} \sum_{n=1}^{N} {N \choose n} \Gamma(M+1) (-1)^{n-1} \int_{0}^{+\infty} \frac{x^{-1/2} \exp[-x(b - \frac{n\lambda_{PS}\lambda_{SD}\Psi_{I}}{2\kappa\Psi_{P}\lambda_{ID}})]}{\sqrt{x}W_{-M,\frac{1}{2}} (\frac{n\lambda_{PS}\lambda_{SD}x\Psi_{I}}{\kappa\Psi_{P}\lambda_{ID}})} dx$$
(28)

With the help of Equation [54][Eq: 7.621.3], we have:

$$\Phi_{2} = \frac{a}{2b\sqrt{\pi}} \sum_{n=1}^{N} {N \choose n} \frac{(-1)^{n-1} \Gamma(M+1) \Gamma\left(\frac{3}{2}\right) \Gamma\left(\frac{1}{2}\right)}{\Gamma\left(M+\frac{3}{2}\right)} \times {}_{2}F_{1}\left(\frac{3}{2}, M+1; M+\frac{3}{2}; \frac{b-\frac{n\lambda_{\text{PS}}\lambda_{\text{SD}}\Psi_{\text{I}}}{\kappa\Psi_{\text{P}}\lambda_{\text{ID}}}}{b}\right), \quad (29)$$

where ${}_2F_1(\alpha,\beta;\gamma;z)$ is the Gauss hyper-geometric function, as defined in section (9.18) of reference [54]. Finally, by alternating (27) and (29) into (26), SER_DSC can be obtained as:

$$SER_{D}^{SC} = \frac{a}{2} - \frac{a}{2b\sqrt{\pi}} \sum_{n=1}^{N} \begin{pmatrix} \binom{N}{n} \frac{(-1)^{n-1}\Gamma(M+1)\Gamma\left(\frac{3}{2}\right)\Gamma\left(\frac{1}{2}\right)n\lambda_{PS}\lambda_{SD}\Psi_{I}}{\Gamma\left(M+\frac{3}{2}\right)\kappa\Psi_{P}\lambda_{ID}} \\ \times_{2} F_{1}\left(\frac{3}{2}, M+1; M+\frac{3}{2}; \frac{b-\frac{n\lambda_{PS}\lambda_{SD}\Psi_{I}}{\kappa\Psi_{P}\lambda_{ID}}}{b}\right) \end{pmatrix}$$
(30)

3.3.2 Scenario 2: MRC Technique Will Be Applied.

By replacing (18) into (25), we get:

$$SER_{D}^{MRC} = \frac{a\sqrt{b}}{2\sqrt{\pi}} \int_{0}^{+\infty} \frac{e^{-bx}}{\sqrt{x}} \times \begin{cases} 1 - \frac{\Gamma(M+N)}{\Gamma(N)} \left(\frac{\lambda_{SD}\lambda_{PS}x\Psi_{I}}{\kappa\Psi_{P}\lambda_{ID}} \right)^{\frac{N-1}{2}} \times \exp\left(\frac{\lambda_{SD}\lambda_{PS}x\Psi_{I}}{2\kappa\Psi_{P}\lambda_{ID}} \right) \\ \times W_{-M-\frac{N}{2}+\frac{1}{2}\frac{N}{2}} \left(\frac{\lambda_{SD}\lambda_{PS}x\Psi_{I}}{\kappa\Psi_{P}\lambda_{ID}} \right) \end{cases} dx$$

$$= \frac{a}{2} - \frac{a\sqrt{b}}{2\sqrt{\pi}} \times \frac{\Gamma(M+N)}{\Gamma(N)} \left(\frac{\lambda_{SD}\lambda_{PS}\Psi_{I}}{\kappa\Psi_{P}\lambda_{ID}} \right)^{\frac{N-1}{2}} \int_{0}^{+\infty} \begin{pmatrix} \frac{N}{2} - 1 \exp\left[-x(b - \frac{\lambda_{SD}\lambda_{PS}\Psi_{I}}{2\kappa\Psi_{P}\lambda_{ID}})\right] \\ \times W_{-M-\frac{N}{2}+\frac{1}{2}\frac{N}{2}} \left(\frac{\lambda_{SD}\lambda_{PS}x\Psi_{I}}{\kappa\Psi_{P}\lambda_{ID}} \right) dx \end{pmatrix}$$

$$(31)$$

By the same approach to claim Φ_2 , Equation (31) can be derived by:

$$SER_{D}^{MRC} = \frac{a}{2} - \frac{a}{2b^{N}\sqrt{\pi}} \times \left(\frac{\lambda_{SD}\lambda_{PS}\Psi_{I}}{\kappa\Psi_{P}\lambda_{ID}}\right)^{N} \frac{\Gamma(M+N)}{\Gamma(N)} \frac{\Gamma(N+\frac{1}{2})\Gamma(\frac{1}{2})}{\Gamma(M+N+\frac{1}{2})} \times_{2} F_{1}(N+\frac{1}{2},M+N;M+N+\frac{1}{2};\frac{b-\frac{\lambda_{SD}\lambda_{PS}\Psi_{I}}{\kappa\Psi_{P}\lambda_{ID}}}{b}).$$
(32)

4. NUMERICAL RESULTS

In this section, we employ the Monte Carlo simulation method to provide numerical results that both validate the accuracy of the proposed analytical frameworks and offer deeper insights into the SER behavior under various key system parameters. The simulation settings and corresponding values are summarized in Table 2.

Figures 3 and 4 illustrate the outage-probability (OP) performance of the proposed system under different values of the transmit SNR Ψ_P and the interference power Ψ_I , respectively, for both SC and MRC combining schemes and two target rates R_{th} . In Figure 3, the OP is observed to decrease monotonically as Ψ_P increases.

Table 2.	Simu	lation	paramete	rs.

Symbol	Parameter name	Value	
R _{th}	Target rate	0.5, 1 (bit/s/Hz)	
η	EH efficiency	0.05 to 0.95	
α	Time-switching ratio	0.05 to 0.95	
$d_{ m PS}$	Distance between P and S	1.5 m	
$d_{ m SD}$	Distance between S and D	2 m	
$d_{ m ID}$	Distance between I and D	0.5 to 5 m	
χ	Path-loss exponent	2.2	
Ψ_{P}	Transmit power-to-noise ratio at P	0 to 50(dB)	
Ψ_I	Transmit power-to-noise ratio at I	0 to 35(dB)	
М	Number of antennas at I	1, 10	
N	Number of antennas at D	1, 10	

This is because a higher transmit SNR improves the received-signal strength, thereby enhancing the achievable data rate and reducing the probability that the instantaneous rate falls below the target threshold R_{th}. Moreover, for the same Ψ_P , the system with a larger R_{th} exhibits a higher OP. This is attributed to the fact that the threshold SNR required for successful decoding, denoted by $\gamma_{th} = 2^{R_{th}} - 1$, increases exponentially with R_{th}. Consequently, the condition $\log_2(1+\gamma) < R_{th}$ (or equivalently $\gamma < \gamma_{th}$) becomes more likely to occur, leading to a higher outage probability. In Figure 4, the OP behavior is examined with respect to the interference power Ψ_1 . As expected, the OP increases as Ψ_1 grows, because stronger interference deteriorates the signal-to-interference-plus-noise ratio (SINR), thereby reducing the achievable rate. Similarly, a higher R_{th} results in a larger OP under the same interference level due to stricter SINR requirements. In all cases, the MRC scheme consistently outperforms the SC scheme, owing to its ability to combine multiple received signals and achieve higher diversity gain, thus improving system robustness against fading and interference. Furthermore, the analytical curves closely match the Monte Carlo simulation results, confirming the accuracy and reliability of the derived theoretical expressions.

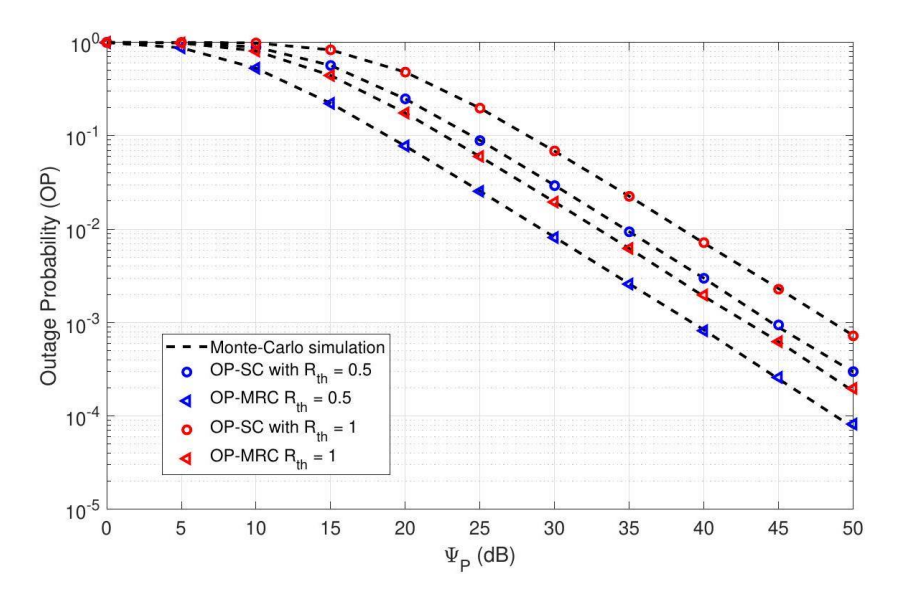


Figure 3. The OP of the proposed system *versus* $\Psi_P[dB]$ with different R_{th} .

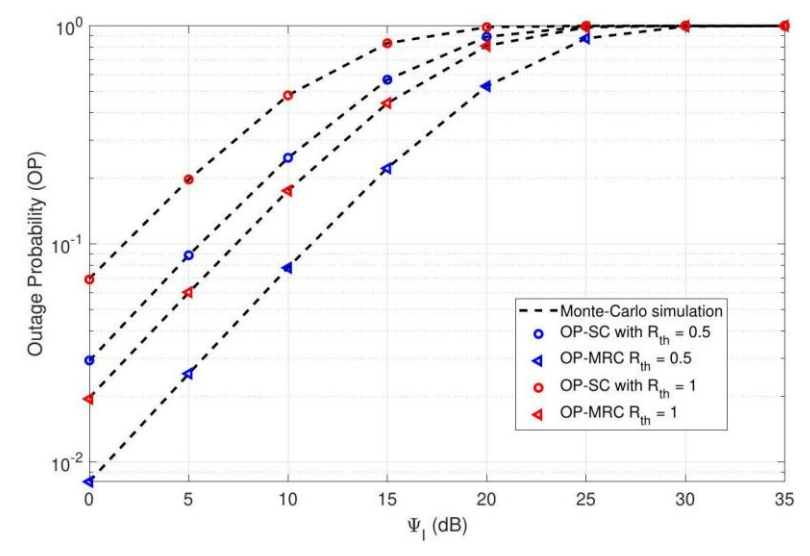


Figure 4. The OP of the proposed system *versus* $\Psi_{\rm I}[{\rm dB}]$ with different $R_{\rm th}$.

Figure 5 illustrates the simulated SER versus the Power Beacon transmit power Ψ_P for different modulation schemes (BPSK, QPSK), combining techniques (SC, MRC), and numbers of receive antennas N at the destination D. The close match between Monte Carlo simulations and analytical results validates the accuracy of the proposed model. As Ψ_P increases, the SER decreases, because the source S harvests more wireless energy from the PB, leading to higher transmit power and improved SNR at D. In the low-to-medium Ψ_P region, the SER reduction is relatively slow, since the system performance is still dominated by CCI. When Ψ_P is sufficiently large, the SER continues to decline, but the marginal improvement becomes smaller if CCI is not mitigated. Comparing SC and MRC, the results show that MRC consistently outperforms SC by achieving better array gain through coherent SNR combining, resulting in downward/leftward-shifted SER curves for the same Ψ_P . Increasing the number of receive antennas from N = 2 to N = 10 further shifts the curves downward and leftward due to higher diversity gain, with the performance improvement being more significant for MRC. Interestingly, under the given system configuration and normalization, QPSK achieves lower SER than BPSK over the entire Ψ_P range. Therefore, for applications requiring both high reliability and high throughput, QPSK combined with MRC and a large N is a promising option. On the other hand, when Ψ_P is limited or CCI is severe, increasing N, employing MRC and/or applying interference-mitigation strategies are effective to avoid the SER floor.

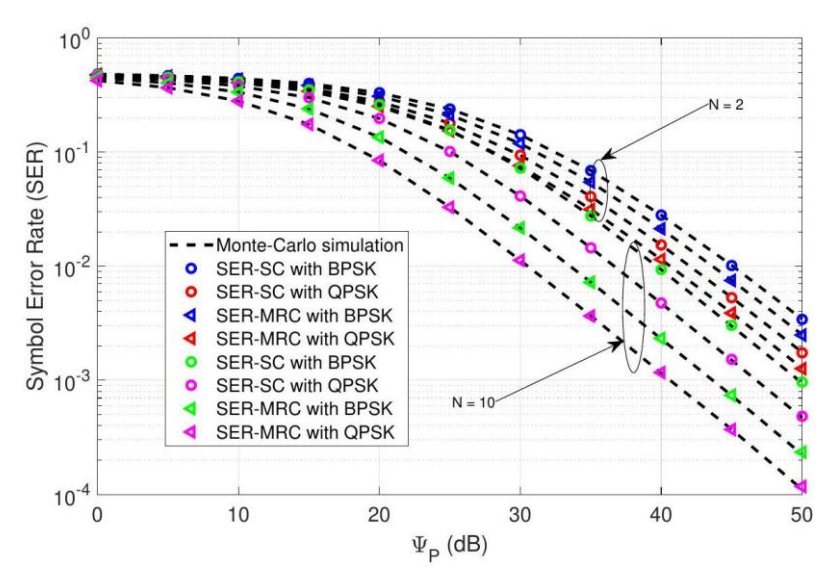


Figure 5. The SER of the proposed system *versus* $\Psi_P[dB]$ with different N.

Figure 6 illustrates the simulated SER versus the interference power Ψ_I at the interfering nodes I for different modulation schemes and combining techniques. As Ψ_I increases, the SER of all configurations rises significantly, because stronger interference reduces the effective SNR at the destination D. In the

low Ψ_1 region, the SER increases relatively slowly, since the signal power from S is still sufficient to suppress interference; however, when Ψ_I exceeds a medium threshold (around 15-20~dB), the curves start to converge and approach a high SER level, indicating an interference-limited regime where further increasing the transmit power of S or improving energy-harvesting efficiency yields little improvement. The relative performance trends between SC and MRC, as well as between QPSK and BPSK, follow the same pattern observed in Figure 5: MRC outperforms SC due to better array gain and QPSK achieves lower SER than BPSK across the entire Ψ_I range.

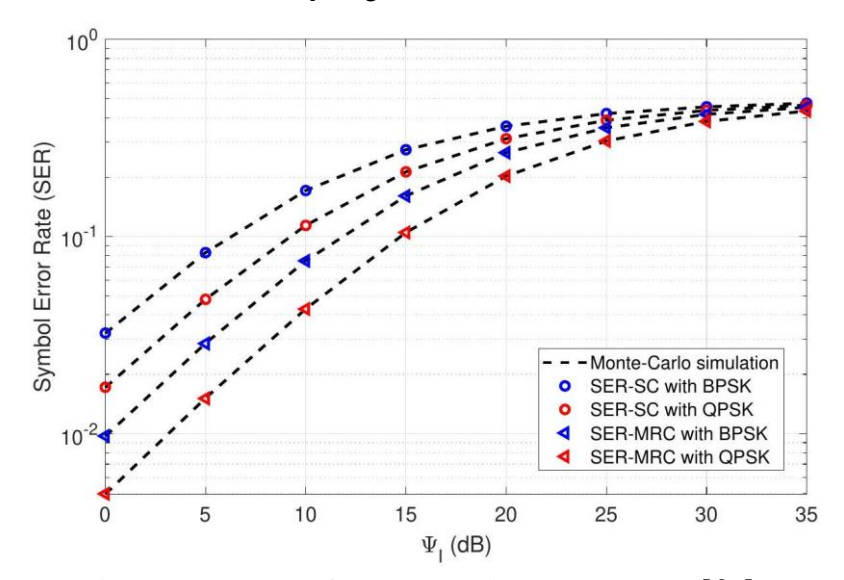


Figure 6. The SER of the proposed system *versus* $\Psi_I[dB]$.

Figure 7 illustrates the simulated SER *versus* the distance $d_{\rm ID}$ from the interferers I to the destination D for different modulation schemes, combining techniques and numbers of interferers M. Based on a simple-path loss model, the mean channel gain can be expressed as $\lambda_X = (d_X)^X$, where d_X denotes the distance between two corresponding nodes and χ is the path loss exponent. Accordingly, as $d_{\rm ID}$ increases, the path-loss term $\lambda_{\rm ID} = (d_{\rm ID})^X$ grows, which causes the interference power received at D to decrease sharply. This reduction in interference directly improves the effective signal-to-interference-plus-noise ratio (SINR) in (30) and (32), resulting in a smaller SER. When $d_{\rm ID}$ is small, the interferers are located close to D and the strong CCI dominates the received signal, leading to a high SER. As $d_{\rm ID}$ increases, the SER decreases rapidly before gradually flattening out when interference becomes negligible. The impact of the number of interferers M is also evident: when M=1, the SER is significantly lower compared to M=10 for the same $d_{\rm ID}$, since fewer interferers contribute less aggregate interference power.

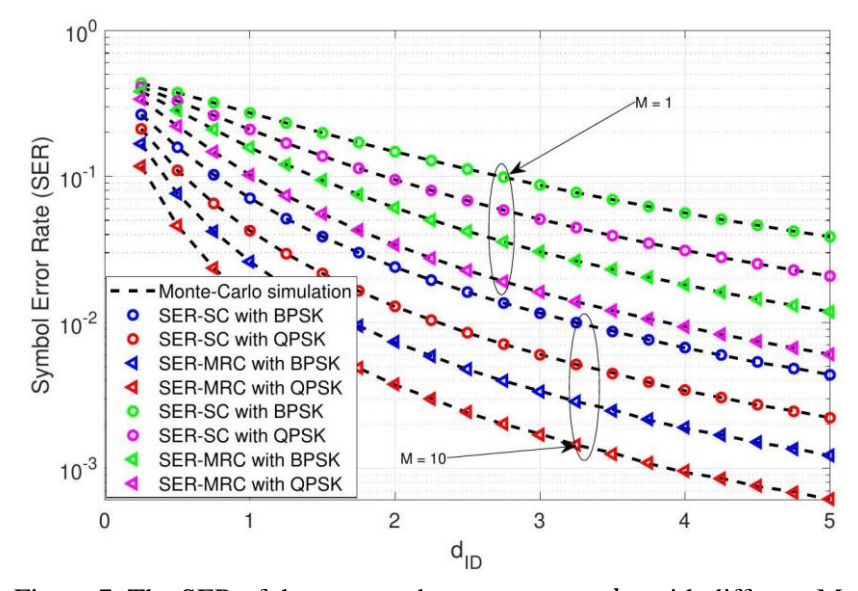


Figure 7. The SER of the proposed system *versus* $d_{\rm ID}$ with different M.

The relative performance trends between SC and MRC, as well as between QPSK and BPSK, remain consistent with previous figures-MRC consistently outperforms SC due to its array gain, while QPSK achieves better SER performance than BPSK, offering improved reliability and spectral efficiency even under interference-limited conditions. These findings highlight the importance of interference management and diversity-reception techniques in maintaining link quality for wireless-powered D2D networks.

Figure 8 presents the simulated SER *versus* the energy harvesting efficiency η for different modulation schemes and diversity combining techniques. As η increases, the SER decreases for all scenarios, because a higher harvesting efficiency allows the relay to collect more energy from the received signals, leading to higher transmit power in the information transmission phase and thus improving the end-to-end SNR. Specifically, increasing η directly enhances the parameter κ in the SINR expressions at the destination, which strengthens the received signal component and consequently reduces the overall SER. The performance gap between SC and MRC remains consistent with previous figures-MRC outperforms SC due to its ability to coherently combine signals from multiple antennas, providing a higher array gain. Similarly, QPSK achieves lower SER compared to BPSK in all cases, as already discussed in earlier results.

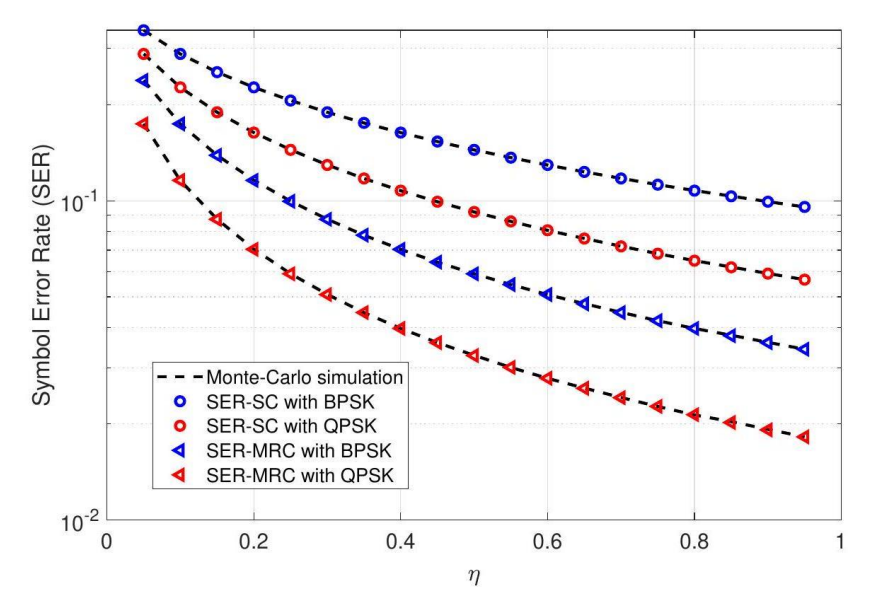


Figure 8. The SER of the proposed system *versus* η .

5. CONCLUSIONS

This work analyzed the SER performance of a wireless-powered D2D communication system with multiple co-channel interferers under a time-switching protocol. Simulation results revealed several key findings. First, MRC consistently outperforms SC due to its coherent combining capability, offering a notable SER reduction across all scenarios. Second, QPSK modulation achieves lower SER compared to BPSK, indicating its advantage in spectral efficiency while maintaining robustness. Third, increasing the energy-harvesting efficiency significantly improves SER, especially at low-to-moderate η values, while greater distances between interferers and the destination lead to substantial interference mitigation. Finally, the system demonstrates high sensitivity to the interference power level, emphasizing the importance of interference-management strategies in energy-constrained D2D networks. Future work could extend the current framework to scenarios with non-identical (i.n.i.d.) power levels and spatial distributions of interferers, providing a more realistic characterization of interference patterns. Moreover, future directions include investigating multiple power beacons with optimized beamforming, integrating ambient backscatter communication to further reduce energy demands, and considering hybrid relay-assisted D2D architectures. In addition, exploring adaptive modulation, interference alignment and machine learning-based resource allocation could enhance system resilience under dynamic spectrum-sharing environments.

REFERENCES

- [1] S. Li, L. D. Xu and S. Zhao, "The Internet of Things: A Survey," Information Systems Frontiers, vol. 17, no. 2, pp. 243-259, 2015.
- [2] K. Rose, S. Eldridge, L. Chapin et al., "The Internet of Things: An Overview," The Internet Society (ISOC), vol. 80, no. 15, pp. 1-53, 2015.
- [3] X. Cui, "The Internet of Things," Proc. of Ethical Ripples of Creativity and Innovation, pp. 61-68, Springer, 2016.
- [4] D. C. Nguyen et al., "6G Internet of Things: A Comprehensive Survey," IEEE Internet of Things Journal, vol. 9, no. 1, pp. 359-383, Jan. 2022.
- [5] J. H. Kim, "6G and Internet of Things: A Survey," Journal of Management Analytics, vol. 8, no. 2, pp. 316-332, 2021.
- [6] G. Gkagkas, D. J. Vergados, A. Michalas and M. Dossis, "The Advantage of the 5G Network for Enhancing the Internet of Things and the Evolution of the 6G Network," Sensors, vol. 24, no. 8, Art. no. 2455, 2024.
- [7] S. C. Mukhopadhyay and N. K. Suryadevara, "Internet of Things: Challenges and Opportunities," Proc. of Internet of Things: Challenges and Opportunities, pp. 1-17, S. C. Mukhopadhyay, Ed. Cham: Springer International Publishing, 2014.
- [8] Y.-K. Chen, "Challenges and Opportunities of Internet of Things," Proc. of the 17th Asia and South Pacific Design Automation Conf. (ASP-DAC), pp. 383-388, Sydney, Australia, 2012.
- [9] T. C. Hung, B. V. Minh, T. N. Nguyen and M. Voznak, "Power Beacon-assisted Energy Harvesting Symbiotic Radio Networks: Outage Performance," PLOS ONE, vol. 20, no. 2, pp. 1-16, Feb. 2025.
- [10] T. C. Hung, Q. S. Nguyen, B. V. Minh, T. T.-Quyen and N. L. Nguyen, "Multi-power Beacon Empowered Secure in IoT Networks: Secrecy Outage Probability Analysis," Advances in Electrical and Electronic Engineering, vol. 23, no. 2, pp. 91-97, 2025.
- [11] T. T.-H. Nguyen, T. N. Nguyen, T. T. Duy, N. H. Son, T. Hanh, B. V. Minh and L.-T. Tu, "Coverage Probability of Energy Harvesting Enabled LoRa Networks with Stochastic Geometry," Journal of Information and Telecommunication, vol. 8, no. 2, pp. 262-279, 2024.
- [12] T. N. Nguyen et al., "On the Dilemma of Reliability or Security in Unmanned Aerial Vehicle Communications Assisted by Energy Harvesting Relaying," IEEE Journal on Selected Areas in Communications, vol. 42, no. 1, pp. 52-67, Jan. 2024.
- [13] D. H. Thuan et al., "Uplink and Downlink of Energy Harvesting NOMA System: Performance Analysis," Journal of Information and Telecommunication, vol. 8, no. 1, pp. 92-107, 2024.
- [14] B. V. Minh, P. T. Tran, T.-H. T. Pham, A.-T. Le, S.-P. Le and P. Partila, "Statistics of the Sum of Double Random Variables and Their Applications in Performance Analysis and Optimization of Simultaneously Transmitting and Reflecting Reconfigurable Intelligent Surface-assisted Non-orthogonal Multi-access Systems," Sensors, vol. 24, no. 18, Art. no. 6148, 2024.
- [15] B. V. Minh, N. H. K. Nhan, T.-H. T. Pham and M. Tran, "Physical Layer Security in Wireless Sensors Networks with Friendly Jammer: Secrecy Outage Probability Analysis," Advances in Electrical and Electronic Engineering, vol. 22, no. 4, pp. 387-398, 2024.
- [16] B. V. Minh, A.-V. Le, V.-D. Phan and T.-H. T. Pham, "Self-energy Recycling in DF Full-duplex Relay Network: Security-reliability Analysis," Advances in Electrical and Electronic Engineering, vol. 22, no. 1, pp. 86-96, 2024.
- [17] H. Balaban and O. Kucur, "Performance Analysis of Energy-harvesting Full-duplex Relaying with Multiantenna and Cooperative Diversity," Proc. of the 2023 3rd Int. Conf. on Mobile Networks and Wireless Communications (ICMNWC), pp. 1-6, Tumkur, India, 2023.
- [18] P. T. Tin, V.-D. Phan, T. N. Nguyen and L. A. Vu, "Performance Analysis for Exact and Upper Bound Capacity in DF Energy Harvesting Full-duplex with Hybrid TPSR Protocol," Journal of Electrical and Computer Engineering, vol. 2021, Art. no. 6610107, 2021.
- [19] D.-T. Vo et al., "Short Packet Communication in IoT Networks: Performance Analysis," Journal of Information and Telecommunication, pp. 1-14, DOI: 10.1080/24751839.2025.2487353, 2025.
- [20] M. S. M. Gismalla et al., "Survey on Device to Device (D2D) Communication for 5GB/6G Networks: Concept, Applications, Challenges and Future Directions," IEEE Access, vol. 10, pp. 30792-30821, 2022.
- [21] N. O. Nwazor and V. K. Ugah, "Device-to-Device (D2D) Data Communications in 5G Networks," International Journal of Advances in Eng. and Manag. (IJAEM), vol. 4, no. 1, pp. 1151-1154, Jan. 2022.
- [22] T. N. Nguyen et al., "On the Performance of Underlay Device-to-Device Communications," Sensors, vol. 22, no. 4, Art. no. 1456, 2022.
- [23] N. T. Nguyen, P. Fazio and M. Voznak, "On the Performance of Power Beacon-assisted D2D Communications in the Presence of Multi-jammers and Eavesdropper," Journal of Advanced Engineering and Computation, vol. 5, no. 4, pp. 254-264, 2021.
- [24] T.-H. T. Pham, N.-T. T. Nguyen, Q.-S. Nguyen, T. Hon, B. V. Minh, Q. S. Nguyen and M. Tran, "Performance Analysis in D2D Partial NOMA-assisted Backscatter Communication," 2025.

- [25] M. R. B. Salim, "A Survey on Essential Challenges in Relay-aided D2D Communication for Next Generation Cellular Networks," Journal of Network and Computer Applications, vol. 216, Art. no. 103657, 2023.
- [26] S. Jayakumar and S. Nandakumar, "Reinforcement Learning Based Distributed Resource Allocation Technique in Device-to-Device (D2D) Communication," Wireless Networks, vol. 29, pp. 1843-1858, 2023.
- [27] W. H. Mahdi and N. Taşpinar, "Bee System-based Self Configurable Optimized Resource Allocation Technique in Device-to-Device (D2D) Communication Networks," IEEE Access, vol. 12, pp. 3039-3053, 2024.
- [28] A. Khan and R. Das, "Security Aspects of Device-to-Device (D2D) Networks in Wireless Communication: A Comprehensive Survey," Telecommunication Systems, vol. 81, pp. 625-642, 2022.
- [29] K. Haseeb, A. Rehman, T. Saba, S. A. Bahaj and J. Lloret, "Device-to-Device (D2D) Multi-criteria Learning Algorithm Using Secured Sensors," Sensors, vol. 22, no. 6, Art. no. 2115, 2022.
- [30] V.-D. Le et al., "Enabling D2D Transmission Mode of Reconfigurable Intelligent Surfaces Aided in Wireless NOMA System," Advances in Electrical and Electronic Eng., vol. 23, no. 1, pp. 32-42, 2025.
- [31] Q.-S. Nguyen, A. U. Le, T. N. Nguyen, T.-T. Nguyen and M. Voznak, "Short Packet Communications for Relay Systems with Co-channel Interference at Relay: Performance Analysis and Power Control," IEEE Access, vol. 12, pp. 63452-63461, 2024.
- [32] L. A. U. Vu, N. T. Tung, T. T. Duy, T. L. Thanh, T. N. Nguyen and N. Q. Sang, "Performance Evaluation of Short-packet Communications of Single-hop System with Presence of Co-channel Interference," Proc. of the 7th Int. Conf. on Research in Intelligent and Computing in Engineering (RICE 2022), pp. 267-271, Hung Yen City, Nov. 2022.
- [33] N. Q. Sang, T. C. Hung, T. T. Duy, M. Tran and B. S. Kim, "Securing Wireless Communications with Energy Harvesting and Multi-antenna Diversity", Jordanian Journal of Computers and Information Technology (JJCIT), vol. 11, no. 2, pp. 197-210, June 2025.
- [34] R. Alrawashdeh, "A Review on Wireless Power Transfer in Free Space and Conducting Lossy Media", Jordanian Journal of Computers and Information Technol. (JJCIT), vol. 3, no. 2, pp. 71-88, August 2017.
- [35] A.-T. Le et al., "Power Beacon and NOMA-assisted Cooperative IoT Networks with Co-channel Interference: Performance Analysis and Deep Learning Evaluation," IEEE Transactions on Mobile Computing, vol. 23, no. 6, pp. 7270-7283, 2024.
- [36] T. N. Nguyen et al., "Outage Performance of Satellite Terrestrial Full-duplex Relaying Networks with Co-channel Interference," IEEE Wireless Comm. Letters, vol. 11, no. 7, pp. 1478-1482, 2022.
- [37] H. Huang et al., "Outage Probability of Energy Harvesting Cooperative NOMA Network with Direct Link," J. King Saud Univ. Comput. Inf. Sci., vol. 37, Art. no. 90, 2025.
- [38] M. Hoang, B. C. Nguyen, N. N. Thang, M. Tran and P. T. Tran, "Performance and Optimal Analysis of Time-switching Energy Harvesting Protocol for MIMO Full-duplex Decode-and-Forward Wireless Relay Networks with Various Transmitter and Receiver Diversity Techniques," Journal of the Franklin Institute, vol. 357, no. 17, pp. 13205-13230, 2020.
- [39] P. T. Tin, T. N. Nguyen, M. Tran, T. T. Trang and L. Sevcik, "Exploiting Direct Link in Two-way Half-duplex Sensor Network over Block Rayleigh Fading Channel: Upper Bound Ergodic Capacity and Exact SER Analysis," Sensors, vol. 20, no. 4, Art. no. 1165, 2020.
- [40] H. Wen, A. M. T. Khel and K. A. Hamdi, "Effects of Co-channel Interference on the Performance of IRS-assisted Communications," IEEE Trans. on Vehicular Tech., vol. 73, no. 7, pp. 10075-10089, Jul. 2024.
- [41] H. Huang, Y. Wei, L. Liang, Z. Yin and N. Zhang, "On the Analysis of Multisource Cooperative Network Assisted by UAV Relays with Co-channel Interference," IEEE Journal on Miniaturization for Air and Space Systems, vol. 6, no. 2, pp. 144-156, Apr. 2025.
- [42] J. Ding, D. Kang, X. Xie, L. Wang, L. Tan and J. Ma, "Joint Effects of Co-channel Interferences and Pointing Errors on Dual-hop Mixed RF/FSO Fixed-gain and Variable-gain Relaying Systems," IEEE Photonics Journal, vol. 15, no. 1, pp. 1-11, Feb. 2023.
- [43] Q.-S. Nguyen, U.-V. Le Anh, T. N. Nguyen, T.-T. Nguyen and M. Voznak, "Short Packet Communications for Relay Systems with Co-channel Interference at Relay: Performance Analysis and Power Control," IEEE Access, vol. 12, pp. 63452-63461, 2024.
- [44] A. Girdher et al., "Second-order Statistics for IRS-assisted Multiuser Vehicular Network With Cochannel Interference," IEEE Trans. on Intelligent Vehicles, vol. 8, no. 2, pp. 1800-1812, Feb. 2023.
- [45] S. Ghose et al., "Jointly Optimal RIS Placement and Power Allocation for Underlay D2D Communications: An Outage Probability Minimization Approach," IEEE Transactions on Cognitive Communications and Networking, vol. 10, no. 2, pp. 622-633, April 2024.
- [46] Z. Li, J. Xing and J. Hu, "Outage Performance of SWIPT-D2D-based Hybrid Satellite-Terrestrial Networks," Sensors, vol. 25, no. 8, Art. no. 2393, 2025.
- [47] Y. Wang, L. Feng, S. Yao, H. Liang, H. Shi and Y. Chen, "Outage Probability Analysis for D2D-enabled Heterogeneous Cellular Networks with Exclusion Zone: A Stochastic Geometry Approach," CMES-Computer Modeling in Eng. and Sciences, vol. 138, no. 1, pp. 639-661, 2023.

"Power Beacon-assisted Energy Harvesting in D2D Network under Co-channel Interferences: Symbol Error Rate Analysis", N.Q. Sang et.al.

- [48] D.-W. Lim and J.-M. Kang, "Joint Transmit Power and Power-splitting Optimization for SWIPT in D2D-enabled Cellular Networks with Energy Cooperation," Mathematics, vol. 13, no. 3, Art. no. 389, 2025.
- [49] R. Nagarajan and N. M. V. Mohamad, "Energy Efficient Rresource and Power Allocation for Uplink Underlay D2D Communication in HetNet-based 5G Network," Journal of Wireless Com. Network, vol. 2025, Art. no. 24, DOI: 10.1186/s13638-025-02452-1, 2025.
- [50] M. Z. Islam and M. N. Adnan, "A Robust Resource Allocation Method for Energy Efficient Device to Device (D2D) Communication," ICCK Transactions on Mobile and Wireless Intelligence, vol. 1, no. 1, pp. 32-39, DOI: 10.62762/TMWI.2025.764788, 2025.
- [51] T. N. Nguyen, P. T. Tran and M. Voznak, "Wireless Energy Harvesting Meets Receiver Diversity: A Successful Approach for Two-way Half-duplex Relay Networks over Block Rayleigh Fading Channel," Computer Networks, vol. 172, p. 107176, DOI: 10.1016/j.comnet.2020.107176, 2020.
- [52] T. N. Nguyen et al., "On Performance of RIS-aided Bidirectional Full-duplex Systems with Combining of Imperfect Conditions," Wireless Netw., vol. 30, pp. 649-660, 2024.
- [53] B. V. Minh, T. N. Nguyen and L.-T. Tu, "Physical Layer Security in Wireless Sensors Networks: Secrecy Outage Probability Analysis," J. of Inf. and Telecomm., vol. 9, no. 1, pp. 1-23, 2025.
- [54] I. S. Gradshteyn and I. M. Ryzhik, Table of Integrals, Series, and Products, ISBN-13: 978-0122947506, Academic Press, 2014.
- [55] D. T. Tam et al., "SER Performance of Millimeter-wave Communications with Multiple Reconfigurable Intelligent Surfaces and Transmit Antenna Selection," AEU-Int. J. of Electronics and Communications, vol. 160, Art. no. 154517, 2023.

ملخص البحث:

تبحث هذه الورقة في الأداء المتعلق بمعدّل خطأ الرّموز في نظامٍ مُشغّلٍ لاسلكياً للاتّصال من جهاز إلى جهاز يعمل تحت بروتوكول تبديل الوقت في ظلّ وجود تداخلات من عدّة قُنوات. ويتضمّن النّموذج المقترح مصدراً يعمل بلا بطّارية يقوم بحصاد الطّاقة من منارات طاقة متعدّد ومن ثمّ يُرسل البيانات إلى هذف متعدّد الهوائيات.

وإلى جانب تحليل معدّل خطأ الرّموز، يتمّ البحث في الأداء المتعلّق باحتمالية انقطاع الطّاقة، بناءً على دوال التّوزيع التّراكمي المشتقة؛ من أجل إضافة منظور آخر في ما يسرتبط بموثوقية النّظام. ويركز التّحليل على آثار عددٍ من المتغيرات الأساسية للنّظام، بما فيها مُستوى طاقة التّداخل، وبُعْد مصدر التّداخل عن الهدف، وفعالية حصادِ الطّاقة، ونوع التّعديل، على الأداء الإجمالي للنّظام.

وتقدم هذه الورقة نتائج محاكاة شاملة؛ بهدف التّحقُّق من الاشتقاقات التّحليلية وبيان تاثيرات المتغيرات سالفة الدّكر على كلٍّ من معدّل خطأ الرّموز، واحتمالية انقطاع الطّاقة. وتوفّر النّتائج النّي تم الحصول عليها فَهْماً معمّقاً لتصميم أنظمة الاتّصال من جهاز إلى جهاز محدودة الطّاقة الّتي تعمل في بيئات تقوم على الاشتراك في الطّيف، بحيث تُعدّ النّتائج الخاصة بهذه الدّراسة مرجعاً للتّحسينات المستقبلية والتّطبيقات العملية.



This article is an open access article distributed under the terms and conditions of the Creative Commons Attribution (CC BY) license (http://creativecommons.org/licenses/by/4.0/).